# An Evaluation of Multicomponent Weft-Knit Twill Structures for Sensing Tensile Force

Roland Aigner and Frank Hepper

***Abstract*—We present multicomponent knit resistive sensors for tracking tensile force. The knits were fabricated using a Twill structure, which is a simple pattern featuring anisotropic elastic behavior, providing high stability along the course direction. Our sensors are made of two commercially available conductive yarn types, with highly different linear resistance. We present a variety of integration methods using the proposed Twill structure, all of which can be easily replicated on a two-bed weft-knitting machine. We evaluate the performance of the resulting sensor variations, with respect to consistency, hysteresis, short-term and long-term relaxation, and drift, among other metrics. We found that particulars of the knit's loop composition have a crucial effect on the consistency of the sensor readings. Furthermore, we show that knitting resistive yarn more tightly than the substrate material gives superior results and that improving elastic recoil by adding Lycra to the supporting substrate can considerably improve performance.**

***Index Terms*— E-textile, force sensor, knitting, resistive sensing, textile sensor, weft-knitting.**
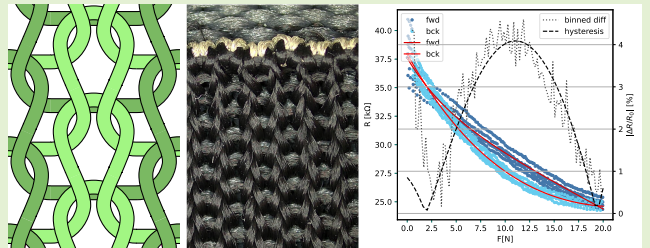
I. INTRODUCTION

TEXTILE-BASED sensors provide beneficial features such as high flexibility and breathability, which can make them comfortable for wearing them on skin, e.g., when compared with foil-based solutions [2], [3], [4], [5]. This is attractive for use cases requiring long duration of direct skin contact, such as therapy scenarios via biomonitoring [6] and activity tracking [7], [8], but also for user interfaces such as data gloves, for tracking of hand posture [9], [10] or gesture detection [11]. Many of those use cases are already implemented with knit fabrics, since they are particularly suitable for sensing strain due to their innate stretchability.

Although there already is a large body of work focusing on knit strain sensors, we found that most of them are based

on highly stretchable fabrics, which are not always desirable. Many scenarios, also beyond garments, require solutions that provide higher tensile stability, or even anisotropic elasticity. Those properties are mostly subject to the geometric composition of the knit, i.e., the knitting pattern. In weft-knitting, those patterns can be thoroughly engineered down to loop level, which is in contrast to warp-knitting [12]. Examples for patterns with relatively high extensibility are plain knit (aka. Single Jersey) [13], [14], [15], [16], [17], Double Jersey [13], and rib structures [13], [18], [19]. In contrast, patterns with higher stability are relatively rare in related literature; examples for those are Interlock used by Atalay et al. [6], and Cardigan used by Ehrmann et al. [20], which showed they provide better sensitivity in low-elongation ranges, when compared with Double Jersey. However, both Interlock and Cardigan represent patterns that occupy both the machine's needle beds at all times, which is a potential limitation in flexibility for fabrication and design. Therefore, and in contrast to the stated works, we use a pattern that is inconsistently called *Twill* in the textile industry, due to its structural similarity with the weave pattern of the same name. It is a generally widespread and simple pattern, however, not touched in textile sensor literature, to our knowledge. As illustrated in Fig. 1(a), it consists of courses of alternating knit and float stitches, while the sequence is shifted by one needle for every other course. Due to this high number floats, it provides exceptional stability in the course direction (i.e., "horizontally"), while being more extensible along the wale direction (i.e., "vertically"), when compared with Plain
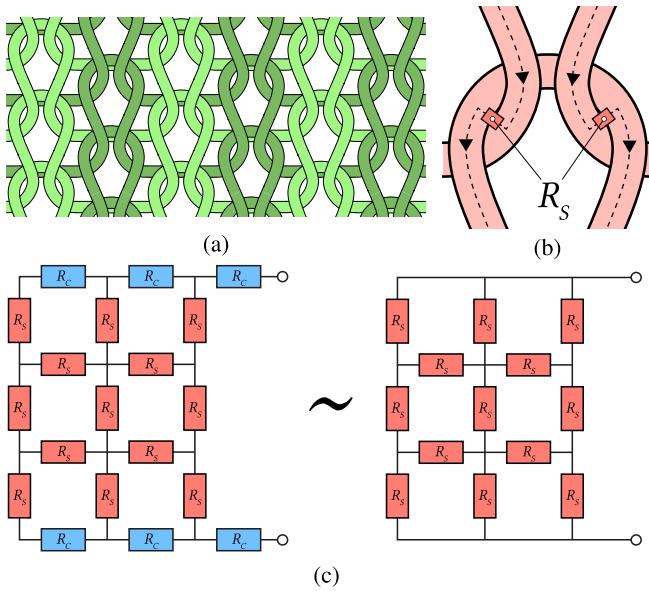
Fig. 1.   (a) Illustration of a Twill knitting pattern. Where current flows along the yarn, loop intermeshing points act as variable resistors (b), increasing conductivity with physical stress at the contact positions. (c) Overall knit geometry can therefore be modeled as a network of variable resistors. We maximize the ratio of sensor yarn resistivity and connector yarn resistivity, so changes in connecting parts' resistance R_C are negligible over the much higher absolute values from sensor loops R_S.

or Double Jersey Knits. This represents a distinct property of a Twill, as opposed to Cardigan or Interlock, with exactly opposite behavior, as a preliminary study confirmed (see supplement). Note that manufacturing of a Twill only requires one needle bed, which increases flexibility and can be a design advantage over other patterns. For example, using a two-bed machine, the entirety of the sensing part can be hidden away to one face of the knit, as done in the work presented in this article, which can be of esthetic preference and/or protect it from exposure and therefore from abrasion and damage.

In contrast to most of the related work, which focuses on sensing strain [9], [13], [17], [18], [21], [22], [23], our primary interest is in sensing *force*, which cannot be trivially inferred from strain directly, due to short-term wear-out effects, exposing hysteresis. Furthermore, knits are subject to considerable structure-dependent relaxation, causing a gradual, nonlinear decrease in force at constant elongation. Based on our observations during this work, we noted that recorded displacement values (and thus inferred strain values) are not entirely adequate to reflect the state of the fabric, since it may be slack when the actuator returns to its initial position. We argue that due to these effects, it would be necessary to record and reconstruct the true fabric lengths by different means, e.g., by optically tracking its geometric state, which would complicate not only the setup but also reporting and its comprehensibility. Within our work, we consequently investigate the sensors' response to force directly and thus avoid this issue. For the sake of comparability with related work however, we still include strain data in this article.

By combining two types of conductive yarn that are knit directly into the fabric, we produce a fully functional textile

force sensor without requiring manual finishing steps. This is opposed to augmenting preexisting knits by embroidering [9] or printing [24] functional parts, or by sewing patches of conductive fabric [25]. Other works demonstrate the method of polymerizing parts of textiles with polypyrrole, e.g., the seminal work of De Rossi et al. [26] showed a data glove with resistive sensing areas. However, this process is challenging to do in a consistent manner, when compared with computerized flatbed knitting, which provides loop-level control. Hence, in contrast to the stated works, our method enables to precisely design and tune the sensor structure even to create highly intricate sensor shapes and complex connector traces (cf. [27]).

The goal of our work was to find the optimal variant with respect to general sensor consistency (for repeated actuation with equal or varying force, as well as different actuation speeds), hysteresis, dynamic range, offset, relaxation, drift, and anisotropic behavior. We therefore explored different implementations and contrasted their behavior in a systematic evaluation.

In a nutshell, the top contributions of this article are as follows.

1) Three methods of integrating a Twill-based resistive sensor on a Twill substrate fabric, including conductive knit connector traces for attaching electronics at remote positions.
2) Ten variations in these sensor designs, using different substrate material compositions and yarn tensions.
3) An in-depth evaluation of those ten variations and our findings regarding consistency, relaxation, offset, and drift in different scenarios.

II. Sensor Implementation

In the following chapter, we outline the sensor design, including potential for slight modifications that we expected to have an impact on sensor performance. We present our knit samples and specify manufacturing details. All our patches were knit on a flat-bed knitting machine of type ADF 530-32 KI W Multi Gauge from KARL MAYER STOLL, at gauge E 7.2. Knitting programs were created with Pattern-software M1 PLUS Version 7.5.

A. General Sensor Design and Sensing Principle

The functional principle of our knit force sensors is according to Holm's theory [28], which states that contact resistance depends on material resistivity ρ and hardness H, as well as contact point count n and pressure P, with

$$R = \frac{\rho}{2}\sqrt{\frac{\pi H}{n P}}.$$

Since contact pressure between loops is varying (and may even be zero when loops lose contact), the resistance drops when force is applied. Consequently, each intermeshing point in the sensor knit can be considered a variable resistor [cf. Fig. 1(b)], and moreover, the overall structure can be modeled as a network of resistors, as done for analytical solutions by [22], [29], and [30].

Similar to Baribina et al. [31] and Semjonova et al. [27], we use a multimaterial sensor layout, combining conductive
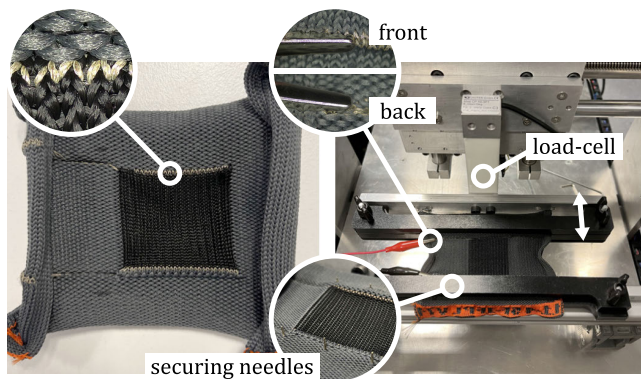
Fig. 2. Sample of one of our sensor patches (left), with conductive yarn traces connecting the resistive area (black) on both upper and lower ends. We evaluated our sensors using a custom-built tensile tester with an integrated force cell (right).

and resistive yarn, i.e., two types with largely different linear resistance, which provides several advantages as follows.

1) Conductive parts can be used to knit connector traces, which enable to comfortably attach readout electronics at remote positions of the fabric. This is unlike other work that requires attaching of connecting wires directly at the sensing structures, such as [8] and [11].

2) In increasing the resistance ratio of sensor area to connector, trace we ensure that the sensor area operates in vastly different absolute value ranges, when compared with the connecting parts. Hence, resistance changes caused by deformation of the connectors are minor and therefore negligible, when compared with the sensor's operational range. This is similar to [31] and addresses an issue often ignored in related work, while furthermore enabling to create more explicit and localized force sensors on a textile.

3) Connecting the resistive part with conductive yarn along the entire width (cf. Fig. 2 left) provides more uniform current flow across all the wales [cf. Fig. 1(c)], since R_C is insignificant against R_S. This should improve sensitivity consistency across the whole sensor area, which could be particularly relevant when the number of sensor wales is much higher than the number of its courses.

B. Materials

As a resistive yarn for the sensor areas, we used Shakespeare Resistat P6204 H100i,[1] which is a den 100/24 polyester fiber with carbon sheath, providing relatively high linear electrical resistance of ∼10 MΩ/m. We twisted four den 100/24 threads with 30S in the first stage and 50Z in the second stage, to achieve adequate yarn count for a balanced knit when combined with our PES yarn, yielding a den 400 thread with den 100/24 × 4 and ∼2.5 MΩ/m.

The conductive traces for providing connections were knit with Shieldex Madeira HC40,[2] which is a silver-coated PA yarn with den 260 and electrical resistance of <300 Ω/m and proved highly durable during previous work [32], [33].

[1] https://shakespeare-pf.com/product/polyester/
[2] https://www.shieldex.de/products/madeira-hc-40/

For the surrounding substrate base structure, we used a PES with den 150/30 (TWD Fibers GmbH). The Lycra that we plated along the PES for improving the fabric's elastic recoil was a den 140 Lycra core covered with PES den 150/20 (Jörg Lederer GmbH).

C. Knit Structure and Manufacturing

As any pattern that is knit on a single bed, internal forces on the Twill are unbalanced, meaning it shows inherent curling tendency. For many use case scenarios, where the knit is tailored together with other parts, this may not be an issue. Otherwise, it can be counteracted by framing with a more stable knit structure.

Instead of implementing the sensor area as an Intarsia field within a surrounding PES structure (cf. [10], [11], [14], [29], and [34]), we knit the resistive yarn on the opposite needle bed and connect it to the PES face, which is knit as a continuous Twill. Apart from a more straightforward integration into a knit, this provides better control about the force distribution throughout the structure. Due to different properties of PES and Resistat, an Intarsia field requires proper tuning of yarn count and stitch settings, to prevent an unbalanced and nonuniform surface. By knitting two faces on opposite beds, we gain more flexibility in tuning the Resistat tightness—and therefore the sensor's responsiveness—without introducing areas of considerable physical, visual, and haptic inconsistency. A side effect is also that the functional parts can be hidden away and are therefore protected from abrasion by the covering PES layer, which may be a benefit in some use cases.

For connecting the sensor face with the base structure, we tuck the Resistat to the opposite bed at the beginning of each knit course. On upper and lower courses, the Resistat is knit to the conductive yarn which provides connector traces. Fig. 3 provides a detailed knitting diagram. For knitting, we plied two threads of den 400 Resistat for the resistive parts, two threads of den 260 Madeira HC40 for the conductive parts, and six threads of den 150 PES for the substrate.

D. Variations

As mentioned above, we knit nonfunctional PES and functional Resistat on opposite needle beds, yielding two knit faces that need to be fixated so they do not fall apart. We investigated three options of doing so: the most straightforward one is to connect both the faces along the sensor's outer wales [cf. Fig. 3(a)], by tucking at the respective outer needles. This results in a "tubular" knit structure, which henceforth will address with "T." Note that both the faces are completely detached in this knit, which could lead to erratic behavior, depending on the fabric's firmness. We therefore tried three variations with the sensor parts knit with different tightness: one with the Resistat knit with *lower* tension than the PES ("Tl"), one with *medium* tension, meaning PES and Resistat tightness balanced ("Tm"), and one with Resistat knit with *higher* tension than PES ("Th").

We furthermore created variations that kept both the faces closely attached, by tucking the Resistat to the PES ("$P \leftarrow R$") across the entire courses [cf. Fig. 3(b)], as well
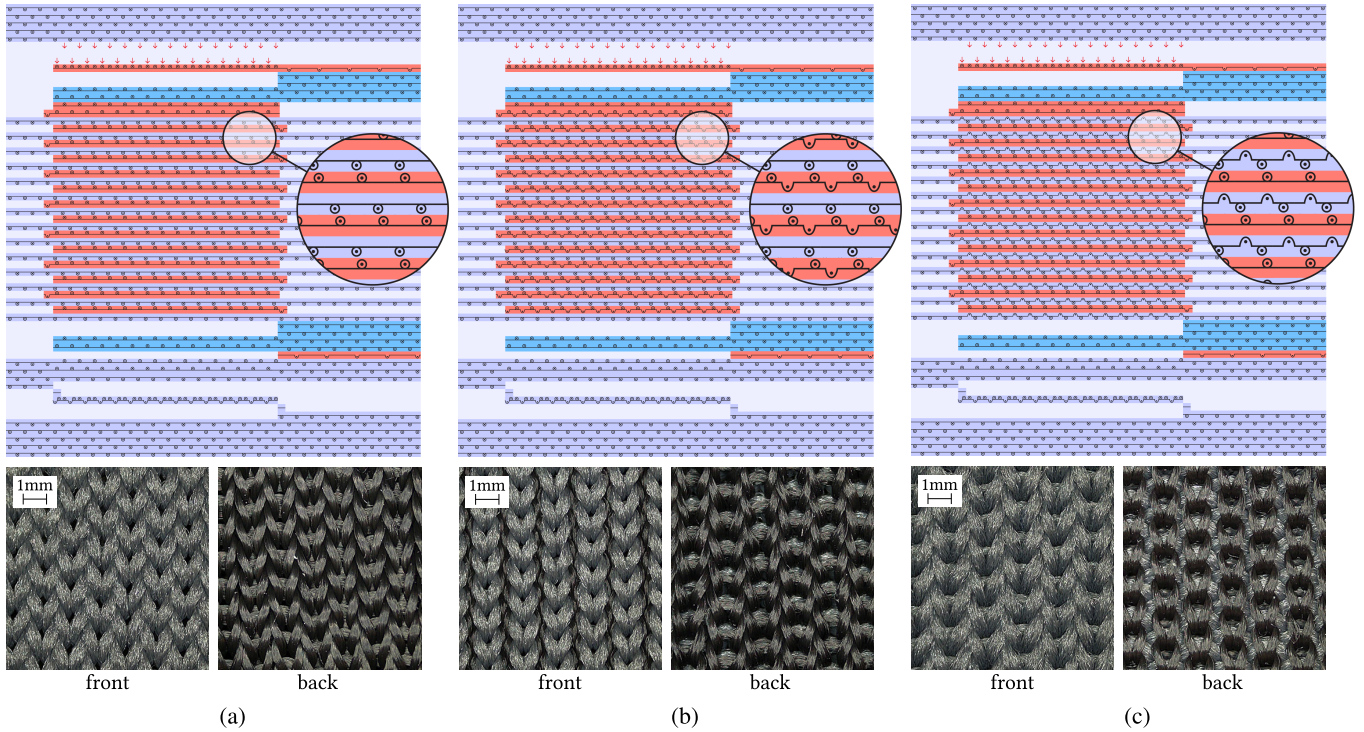
Fig. 3.   Twill-based knitting structures for (a) *T* (tubular), (b) *P ← R* (Resistat tucked to front-face PES), and (c) *P → R* (PES tucked to back-face Resistat). Note the connecting front bed tucks at the beginning of each Resistat row (red) which secures the edges of the sensor area with the substrate knit (purple). Connector traces (blue) are knit on the back bed for connecting to the Resistat loops, and on the front bed otherwise. Images at the bottom show closeups of front bed (PES) and back bed (Resistat) faces of the resulting knit structures. In particular, the closeups show (a) P_{Tm}, (b) P_{RP}, and (c) P_{PR}.

TABLE I
OVERVIEW OF OUR SENSOR VARIATIONS. WE VARIED STRUCTURE COMPOSITION (TYPE), RATIO OF PES THREADS VERSUS LYCRA THREADS, NOMINAL STITCH LENGTH (NP) OF SUBSTRATE MATERIAL (PES + LYCRA), RESISTAT MATERIAL (RES), AND TUCK STITCHES THAT CONNECT FRONT AND BACK FACES. NOTE THAT NP IS A MEASURE OF YARN USAGE PER LOOP, I.E., LOWER NUMBERS REPRESENT TIGHTER KNITS

Name	Type*	PES	Lycra	NP PES	NP Res	NP tuck	notes
P_{Tl}	T	6	-	13.1	13.5	-	tubular, low tension for Resistat
P_{Tm}	T	6	-	13.1	12.5	-	tubular, medium tension for PES/Resistat
P_{Th}	T	6	-	13.1	11.5	-	tubular, high tension for Resistat
P_{RP}	P←R	6	-	13.1	12.0	9.0	Resistat tucked to PES
P_{PR}	P→R	6	-	13.1	12.0	9.0	PES tucked to Resistat
$PL1_m$	P→R	5	1	12.5	12.5	9.0	1×Lycra + medium tension Resistat
$PL1_h$	P→R	5	1	12.5	11.5	9.0	1×Lycra + high tension Resistat
$PL1_{ml}$	P→R	5	1	12.5	12.5	9.5	1×Lycra + medium tension Resistat, low tension tuck
$PL2_{m+}$	P→R	4	2	12.0	11.8	9.0	2×Lycra + medium-high tension Resistat
$PL2_{hl}$	P→R	4	2	12.0	11.5	9.5	2×Lycra + high tension Resistat, low tension tuck

* Types: T = tubular knit; P←R = Resistat is tucked to front-face PES; P→R = PES is tucked to back-face Resistat

as the opposite, tucking the PES to the Resistat loops ["*P → R*," cf. Fig. 3(c)].

From handling with the resulting knits, we could subjectively see that our first variations with six threads of PES ("*P*") were prone to short-term wear-out and we therefore expected poor elastic recoil. For this reason, we also created samples that combined PES with Lycra ("*PL*"), to encounter this aspect (cf. Table I). Hence, in addition to using 6 × PES for the surrounding substrate, we also created patches where we plated 5 × PES together with 1 × Lycra ("*PL1*"), as well as 4 × PES with 2 × Lycra ("*PL2*"). We already saw during our first evaluation that lower tension Resistat patches performed poorly, as well as connecting front and back faces outperform tubular structures, and we therefore chose to focus on those for our Lycra variations, hence all of them were knit of type *P → R* with *medium* to *high* Resistat tension.

III. EVALUATION

A. Apparatus

For evaluation, we used a custom tensile tester, which we built from an obsolete CNC milling machine (cf. Fig. 2 right). The machine was operated by Art-Soft Mach4 CNC Control Software (v4.2.0), running on a Windows 10 PC. We attached mounts to clamp the textiles on both the ends, incorporated needles at 2-cm distance, and secured the textile so it would not slip. The clamp attached to the moving part was equipped with a single-point load-cell of type Sauter CP P1-Ba-d-1810[3] which was sampled at ∼80 Hz with an ADS 1231 24-bit Delta–Sigma ADC.[4] We acquired the sensors'

[3]https://www.kern-sohn.com/shop/en/measuring-instruments/measuring-cells/CP-P1/
[4]https://www.ti.com/product/ADS1231

resistance values using a simple voltage divider with a reference resistor of 606 kΩ and sampled using an Adafruit ADS1115 16-bit ADC[5] at ~128 Hz. At ~40 Hz, we averaged the samples of the previous period and captured the results into CSV files for later analysis, along with timestamp and actuator displacement. Sampling, recording, and remote control of Mach4 via RS232 were performed by an ESP32 on an Adafruit HUZZAH32 Feather board.[6]

Note that our tensile tester is able to move along three axes, which enables testing for shearing effects; however, this would require a modification for omnidirectional force measurement. Although this would greatly complicate the procedure and evaluation, we see potential for future work, to simulate more generic actuation which may be closer to many real-life scenarios. Since this work focuses on variations in knit structures, we explicitly performed orthogonal actuation in our tests.

B. Procedure

All our knit sensor variations share a similar design (cf. Fig. 2 left), i.e., a 4 × 4 cm square field of resistive yarn, which is connected to conductive traces along the entire upper and lower courses. These connector traces were knit beyond the sensor area, leading to the edge of the textile sample, where we attached crocodile clips to connect our measurement electronics. We chose strong clips to avoid their slipping during the procedure and ensured adequate overlap with the conductive yarn. We refrained from testing different sensor dimensions, since we know from [35] that sensor resistance is directly proportional to height and inversely proportional to width, with $R = \rho(h/w)$, where ρ is a material-specific constant. We were able to verify this correlation in a preliminary evaluation (see supplementary material).

Each sensor variation was knit three times. We performed an *ex ante* evaluation to get an estimate regarding consistency and to identify outliers. We found good consistency overall and a very low number of outlier sensors (see supplement). We did, however, not perform an in-depth formal evaluation regarding consistency at this point.

For each sample, a single five-cycle procedure was recorded. For the testing procedure, we marked the textiles at 5-cm distance with the 4-cm sensor areas centered, giving 5 mm extra on each side for mounting. The samples were then punched through the mounting needles at the marks, so the tests would start from consistent initial lengths of 5 cm. Tested patches were not previously ironed or otherwise chemically, mechanically, or thermally treated.

1) Pulling With Equal Force: To observe correlation of sensor reading and applied force, as well as sensor offset and general consistency, we performed a test procedure repetitively applying force along the wale direction and releasing again. We chose the force based on an informal initial test, where we estimated the upper working limit of most of our sensor variants with ~20 N and repeated for five cycles with a jog rate of 1.333 mm/s. Note that due to a communication

lag in between the ESP32, Mach4, and the testing machine, we were slightly overshooting the target forces, however, this does not undermine the general point of our results. Also note that since different samples had different elastic behavior, this resulted in different strain ranges. Moreover, since we are not observing strain but force, we returned to $F = 0$ N after each cycle, which does not align with the initial actuator position of $d = 0$ mm, due to fabric extension from wear-out. As a result, this offset in strain could be considered a metric for the fabric's wear-out.

2) Pulling With Dwell: To investigate drift and relaxation effects, we conducted a test similar to our initial one; however, instead of switching actuation direction at 20 and 0 N immediately, we dwelt for 5 s at each position. Note that due to ongoing fabric relaxation, the force was not constant at this point. We refrained from readjustment motions, since we judged this would introduce considerable jerkiness in the data and complicate analysis.

3) Pulling With Varying Speed: Since we noted during *ex ante* experiments, that actuation speed can have a profound impact on the sensor reading—most notably on the spikes in resistance after starting and stopping—we repeated our initial tests (five cycles at 20 N, no dwell) with half and twice the baseline speed; hence, speeds were 0.667, 1.333, and 2.667 m/s.

4) Pulling With Increasing Force: To find the upper sensing range limit and to inspect consistency when pulled with different amplitudes, we varied pulling force. For this test, we started at an initial 5 N and increased in steps of 5 N up until 40 N, with returning to 0 N after each cycle. The test was again based on our initial one, i.e., we did not dwell before switching direction and moved with 1.333 m/s.

5) Long-Term Pull: To observe long-term drift and relaxation effects, we performed a test pulling the samples to 20 N and returning to 0 N, dwelling for 15 min at each end.

6) Course-Directional Pull: In related work, knit strain sensors are frequently tested along a single direction [13], [18], [22]. However, like most knitting structures such as Jersey and Rib patterns, a Twill is subject to anisotropic behavior in terms of physical properties, such as elasticity and recovery. We therefore investigated the behavior orthogonal to our primary testing direction as well, by mounting the sample rotated accordingly in our testing apparatus.

IV. Results and Discussion

In the following, we summarize our main findings. Note that to save space and reduce complexity, we narrow down our subset of evaluated patches, by progressively excluding poorly performing sensor variations. Refer to Table II, which sums up the majority of our results.

A. General Performance

1) Non-Lycra Variants: Non-Lycra variants show almost linear relationship between strain e and applied force F for the pulling segments [cf. Fig. 4(a)]; however, during release phase, we see considerable lag throughout all the variations, which is due to poor elastic recoil. This effect inherently translates

---

[5]https://www.adafruit.com/product/1085
[6]https://www.adafruit.com/product/3405

TABLE II

MAJORITY OF OUR RESULTS ARE GATHERED IN THIS TABLE. NOTE THAT WE PROGRESSIVELY EXCLUDED SENSORS THAT WERE PERFORMING BADLY FROM SUBSEQUENT EVALUATION STEPS. BEST VALUES FOR NON-LYCRA AND LYCRA VERSIONS ARE PUT IN BOLD

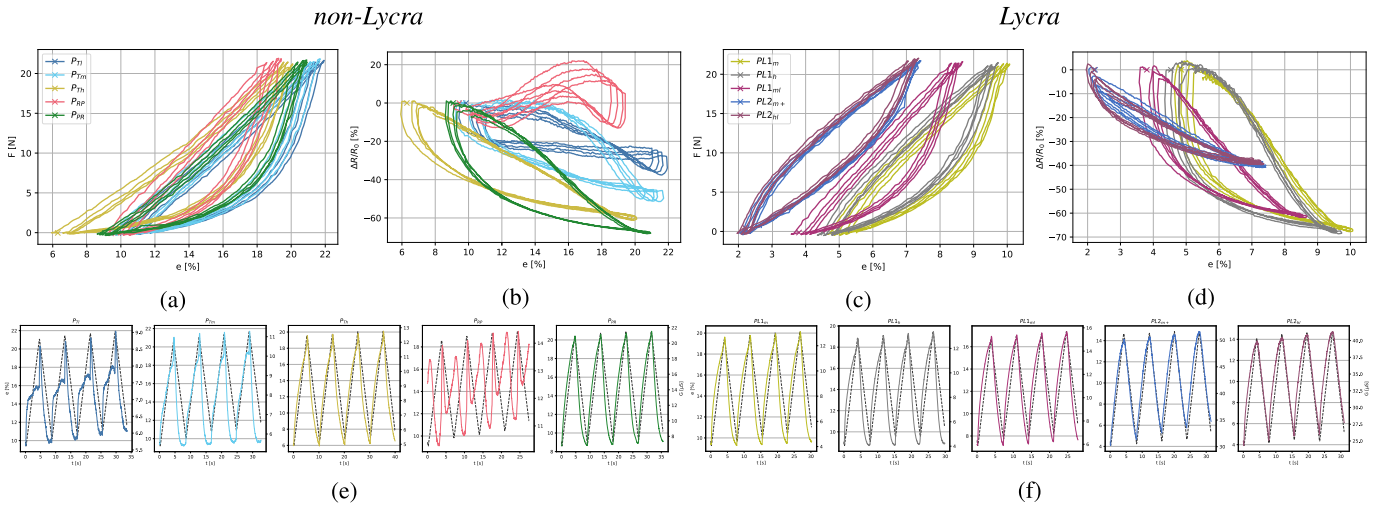|	non-Lycra					Lycra				
	P_{Tl}	P_{Tm}	P_{Th}	P_{RP}	P_{PR}	$PL1_m$	$PL1_h$	$PL1_{ml}$	$PL2_{m+}$	$PL2_{hl}$
$\Delta d_{0,5}$ [%]	11.7	11.8	**7.9**	11.4	10.2	11.0	10.6	9.1	5.4	**5.2**
$\Delta d_{1,5}$ [%]	2.3	2.6	2.0	2.3	**1.6**	1.8	1.9	2.0	**1.3**	**1.3**
r^2	0.65	0.90	**0.91**	-1.94	0.90	0.92	0.90	0.91	0.92	**0.93**
h_R [%]	14.9	27.1	**10.7**	-	25.4	45.6	63.3	24.8	5.8	**4.1**
F_h [N]	0.5	0.0	0.0	-	0.0	0.0	0.0	0.0	9.2	11.1
ΔR_{rel} [%]	24.6	46.5	56.7	-	**64.0**	63.1	**65.9**	56.7	35.4	34.5
offset [%]	-	-	**-1.62**	-	-2.14	-1.62	-	-	-3.45	**-3.24**
relaxation [%]	-	-	7.32	-	**5.80**	-	-	-	2.59	**2.45**
drift [%]	-	-	**23.29**	-	30.38	-	-	-	8.51	**7.93**
T_r [s]	-	-	22.9	-	630.4	-	-	-	**15.1**	**15.1**
T_d [s]	-	-	24.6	-	**23.7**	-	-	-	10.7	*10.2*
jog x 0.5 r^2	-	-	0.84	-	**0.94**	-	-	-	**0.92**	0.20
jog x 2.0 r^2	-	-	**0.90**	-	0.87	-	-	-	**0.94**	0.84
course-dir h_G [%]	-	-	**4.3**	-	8.7	-	-	-	-	-
F [N]	-	-	6.9	-	5.5	-	-	-	-	-

non-Lycra   *Lycra*

Fig. 4. Characteristics and timelines of non-Lycra (left) and Lycra (right) variants: plots of correlation between (a) and (c) strain e and force F, as well as (b) and (d) strain and relative resistance change $\Delta R/R_0$. "x" marks initial values at beginning of recording. (e) and (f) Timeline plots of all variations, overlaying strain e (dashed, black) and sensor conductivity G, show respective conformity of our variations.

into hysteresis in sensor characteristics [cf. Fig. 4(b)], since releasing does not reflect in the knit mesh immediately and instead exhibits notable delay for recovery of the structure. We consider this an innate limitation of knits; however, this can be counteracted to some degree, which was our main motivation to add Lycra into the supporting base knit, as outlined in Section II-D.

We noted that the resting state (i.e., at $F = 0$ N) of the sensor is highly different from the remaining iterations, hinting toward sensor offset. To quantify this wear-out effect, we calculated the relative extension $\Delta d_{0,5}$, i.e., the change in length in between *before* first and *after* fifth pulling iteration. We see that for the non-Lycra variants, P_{Th} performs best, with 7.9% extension. However, the first pulling iteration can be considered an outlier and may be irrelevant in many use case scenarios, e.g., when the fabric is draped and therefore permanently stretched. Therefore, we also report relative extension $\Delta d_{1,5}$, which excludes the first iteration by calculating relative length change in between *after* first and fifth pulling iterations. There, the results are different, with P_{PR} clearly outperforming P_{Th}.

When comparing sensor response by relative change in resistance $\Delta R/R_0$ [cf. Fig. 4(b)], we see that for tubular structures (i.e., P_{Tl}, P_{Tm}, and P_{Th}), tighter knit Resistat areas result in superior characteristics (i.e., P_{Th}, with better correlation between strain and resistance change, less hysteresis, less noisy signal). Unexpectedly, there is considerable difference between the two connected variants P_{RP} and P_{PR}. While the patch with PES tucked to the Resistat ($P \rightarrow R$) clearly outperforms its tubular equivalent P_{Tm}, tucking the other way around ($P \leftarrow R$) results in a defective sensor. We can eliminate the possibility of manufacturing flaws, since all our three specimen of type P_{RP} showed this erratic behavior. We exclude P_{RP} from further evaluations, due to the bad performance.

The difference in sensor performance is also clearly visible on the timeline plots [cf. Fig. 4(e)], where conductivity G of P_{Th} and P_{PR} goes well in line with strain e. Note that since we alternate between 0 and 20 N, the values of e drift slightly upward due to wear-out effects. As mentioned above, we present strain-related data in the article for sake

of comparability; however, we refer the interested reader to the supplement, which shows that the conductivity is well in line with the amplitude of force F in most variations. We quantify conformance between the two trends of F and G using the coefficient of determination[7] $r^2 = 1 - SS_{res}/SS_{tot}$, where SS_{res} is the residual sum of squares and SS_{tot} is the total sum of squares. Both the data series are first normalized using the `preprocessing.StandardScaler` from Python package scikit-learn,[8] which transforms all the values with $y = (x - \mu)/\sigma$. The results show that P_{Tm}, P_{Th}, and P_{PR} perform best in that regard.

2) Lycra Variants: From Fig. 4(c), we see that elastic recoil was slightly improved by adding Lycra; however, the striking linearity we observed for the pulling segments earlier seems to suffer from the boost in elasticity in general. For all the Lycra variants PL*, conformity between force and conductivity is also slightly improved [cf. Fig. 4(f), and r^2 values]. Most notably the variants with $2 \times$ Lycra (PL2*) show best linearity in e/R correlation with least hysteresis [cf. Fig. 4(d)]. Drift also appears to be less severe for those variations, which also reflects on relative extension values $\Delta d_{0,5}$ and $\Delta d_{1,5}$ (cf. Table II).

B. Hysteresis and Dynamic Range

To objectively compare hysteresis, we separated data into pulling and releasing segments and fit exponential functions to the datasets using SciPy function `optimize.curve_fit` (for further details, refer to the supplementary material).[9] We excluded the first pull/release cycle as an outlier for this curve-fitting procedure and normalized R values by scaling with $1/R_0$. We then searched for positions of maximum distance between pulling and releasing curves. The results are reported in Table II, with resistance hysteresis h_R, at respective locations F_h. We see that the variants with two Lycra threads PL2* outperform all others, including non-Lycra knits. Furthermore, their maximum hysteresis is found at $F \sim 10$ N, unlike most patches, which show considerable differences at 0 N, as results of strong settling effects.

We report dynamic range as relative difference in sensor resistance in between $F = 0$ N and $F = 20$ N, i.e., $\Delta R = abs(R_0 - R_{20})/R_0$. To find R_0 and R_{20}, we used the curves fit for finding hysteresis and evaluated them at $F = 0$ N and $F = 20$ N: for non-Lycra versions, the connected sensor shows higher range than the tubular knits. The versions with two strands of Lycra PL2* show least range.

Even though the PL2* variants were inferior in terms of range, we decided to exclude PL1* sensors for further evaluation, since we judged low hysteresis and better consistency far more important than range. We furthermore tried to keep a balanced set of Lycra and non-Lycra patches with the two best-performing each.

C. Offset, Relaxation, and Drift

We use the terminology of [36], with *offset* being the change in resting-state resistance after each pulling iteration, *relaxation* being the continuous change in resistance at constant strain, and *drift* being the continuous change in resistance when returned to resting state. We calculate offset as relative change in resistance between *before* and *after* each cycle. To quantify relaxation and drift, we calculated resistance change relative to the initial value of the respective dwelling segment. For calculating all the three metrics, we again excluded the first pull/release iteration for each sets, since sensors initiate from long-term settled states [cf. initial trends in Fig. 4(e) and (f)]; averaged values of the remaining four segments are presented in Table II.

Offset values show the remaining non-Lycra variants are superior to our Lycra versions. Furthermore, the tubular structure P_{Th} outperforms the connected version P_{PR}. However, tests with dwelling at 0 and 20 N for 5 s each showed that Lycra variants are by far superior in terms of both relaxation and drift, as can be seen also in Fig. 5 (left). For Lycra variants, PL2$_{hl}$ is only slightly superior, while non-Lycra versions tie for both the metrics: the tubular sensor shows less drift but worse relaxation behavior.

The results from long-term test (cf. Fig. 5, right) show similar results. It is clearly visible that P_{PR} exhibits highest relative noise and P_{Th} shows lowest. To compare settling of conductivity values, we calculated RSD over time windows of the past 10 s with $RSD_{10}(t) = \sigma_{10}(t)/\mu_{10}(t)$, where σ_{10} and μ_{10} denote the SD and arithmetic mean of G values in the period $[t - 10$ s$, t]$ respectively. In Table II, we specify periods for RSD_{10} to *permanently* drop below 1%. We report one value for relaxation (i.e., when the sensor patch is pulled, T_r) and one for drift (i.e., after sensor patch is released again, T_d). Similar to our short-term dwelling tests, we observed that both the Lycra variants are by far superior for both relaxation and drift. Furthermore, the Lycra versions' advantage is backed by long-term actuation tests, straining the sensors 2200 times with $e = 20\%$ over a timespan of 5.6 h (see supplement).

D. Actuation Speed

To compare recordings with different lengths resulting from different jog rates, we again discarded the first pull/release iterations as outliers, normalized along time axes, and downsampled our data to equal sample count with `scipy.interpolate.interp1d`.[10] We again scaled our samples using `sklearn.preprocessing.StandardScaler` with $y = (x - \mu)/\sigma$, this time not individually for each recording, but using μ and σ of our baseline set (1.333 mm/s) for all the three speeds, to preserve relative deviations. We then determined conformity of half and double speed from the baseline set by calculating r^2, which can be found in Table II.

We see that for the non-Lycra versions, P_{Th} deviates more for half speed, however less for double speed. For

---

[7]We use the less common lower case notation to mitigate confusion with electrical resistance R.

[8]https://scikit-learn.org/stable/modules/generated/sklearn.preprocessing.StandardScaler.html

[9]https://docs.scipy.org/doc/scipy/reference/generated/scipy.optimize.curve_fit.html

[10]https://docs.scipy.org/doc/scipy/reference/generated/scipy.interpolate.interp1d.html
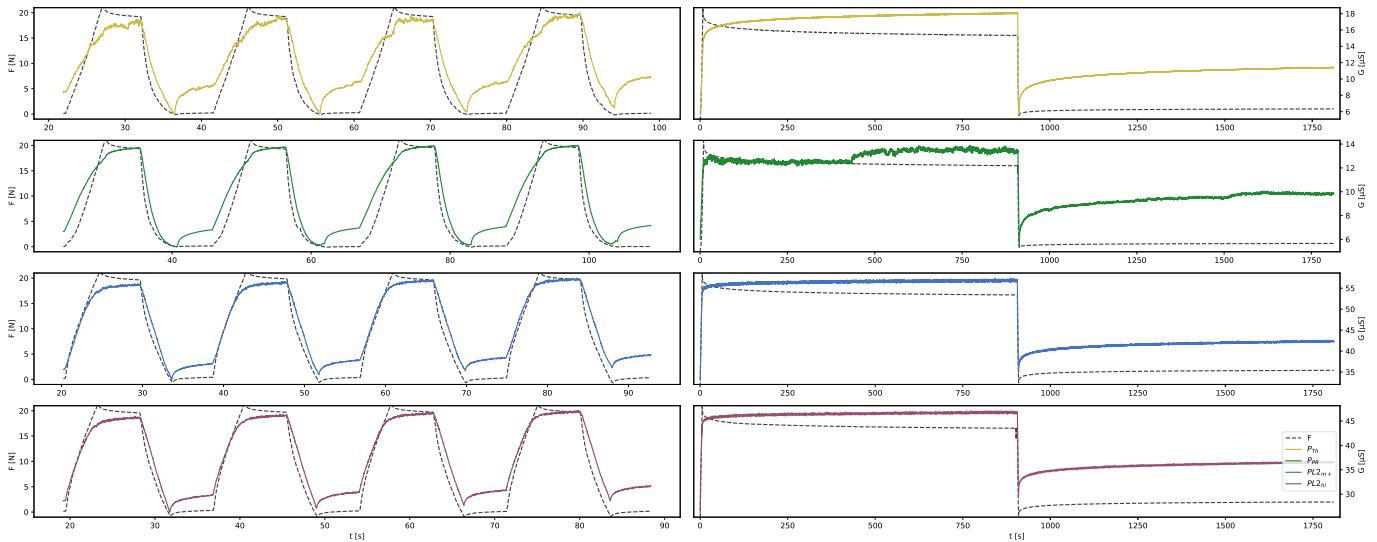
Fig. 5. Results from short-term dwell with repetitive actuation (left) and long-term dwell with single actuation (right) show all sensors are subject to relaxation and sensor drift.
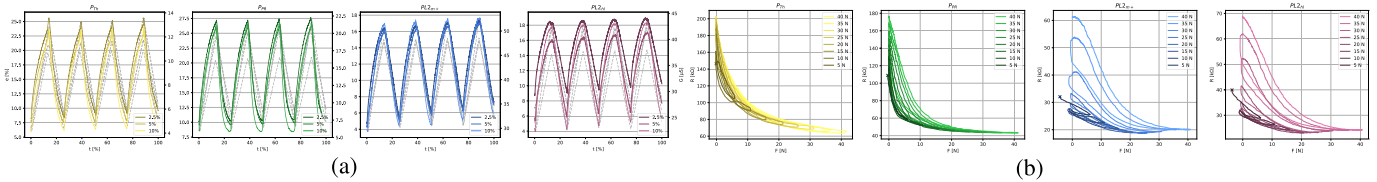

Fig. 6. Results of our jog-rate test (a) showed that PL2$_{m+}$ is most immune against variations in actuation speed. Cascading tests (b) showed that characteristic lines of Lycra variants follow largely different trends, depending on the force applied.

Lycra patches, we see clearly that PL2$_{m+}$ is superior to PL2$_{hl}$ [cf. Fig. 6(a)], which implies that tighter tuck tension (i.e., tighter connection between front and back faces) should be preferred.

E. Increasing Force

Fig. 6(b) shows data collected from continuously increasing force for each iteration in steps of 5 N. We see that both the Lycra variants perform very poorly and follow a different trend for each repetition, returning to largely different sensor values when released. Note that this is most severe when we went beyond our previous upper testing limit of 20 N. Non-Lycra patches show much more consistent trends, with P_{Th} achieving the best results, even in highly strained states. We see furthermore that P_{PR} seems to reach saturation more quickly.

F. Anisotropy

Our main testing direction so far was along wales, where the knit provides good stability. Many use cases cause actuation along a single direction; however, given the anisotropic nature of most knitting structures, it is reasonable to also consider the orthogonal direction. Although for our Twill structure equal force causes higher strain in the course direction, first observations with non-Lycra patches did not hint toward considerable differences in terms of e/R correlation. Our tests, however, show that the Lycra variants exhibit significant erratic behavior when actuated along courses. In particular, characteristics and timelines in Fig. 7 show erratic sensor values for Lycra variants, similar to P_{RP}, which we discarded earlier. We therefore
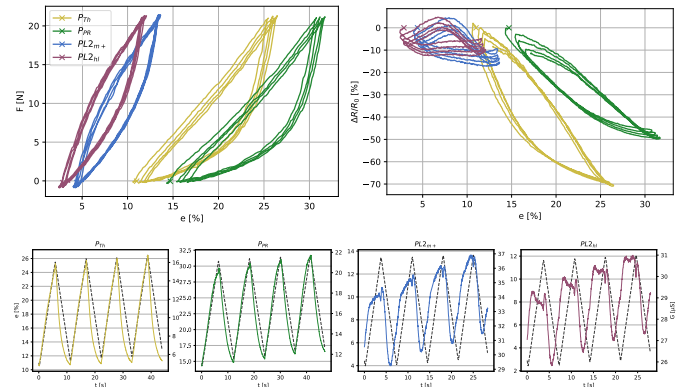

Fig. 7. Course-directional strain behavior is most consistent for non-Lycra variants, while Lycra versions act highly erratic.

infer that patches with Lycra additives are only of limited value for use cases that involve omnidirectional strain and/or shear. Hysteresis data for non-Lycra patches can be found in Table II. As earlier with P_{RP}, we refrained from calculating hysteresis for Lycra variants since we found curve-fitting unreasonable due to their overall erratic behavior and high offsets in between pulling iterations; more details on curve fitting and hysteresis can be again found in the supplementary material.

G. Discussion

Summarizing, we found that when manufacturing our sensors as tubular knits, the resistive part should exhibit slightly higher tension than the substrate. Connecting front and back

faces can yield better results in many instances; however, an unexpected finding was that the tucking direction is crucial: if the resistive yarn is tucked to the substrate, the resulting sensor is defective. If, however, the tucks are performed the other way around, the result is among the best-performing sensors; it, however, gives noisier values when compared with the tubular versions. Lycra variants produced more consistent results overall, at least within our testing range of 0–20 N. They subjectively showed less wear-out effects and better elastic recoil. In terms of quantitative measures, they are less prone to relaxation and drift, both in short- and in long-term. Knit using two threads of Lycra for the substrate showed best linearity, least hysteresis, and is least affected by variations in actuation speed; using higher tuck tension yielded slightly better results.

Still, we see that the best choice of materials depends largely on the specific use case at hand. We noted that Lycra-enhanced variants perform well for wale-directional strain; however, the results were sobering when we varied actuation amplitudes, especially beyond our usual testing range with huge offsets as there was considerable offset and hysteresis visible in the plots. In contrast, the PES-only patches show much less anisotropic behavior and could be used even beyond 20 N, in particular the tubular version P_{Th}.

V. CONCLUSION

In this article, we presented three means of fabrication for implementing a resistive force sensor in flatbed weft knitting machines with a minimum of two beds. The chosen knitting pattern enables to knit the sensing part on one bed entirely, which allows for combinations with a supporting substrate. Our method therefore provides the possibility to hide away the functional part for esthetic and/or protective purposes. Based on these methods, we presented and evaluated ten variations, five of which used a PES-only substrate material. The remaining five combined PES with Lycra to improve their physical properties.

We do acknowledge a few limitations of this study: first, we did not evaluate all possible combinations of nominal stitch numbers (cf. Table I), instead we chose settings driven by subjective measures of quality. We did this to keep the number of patches reasonably low. We did, however, experiment with other compositions and plies which were moderately successful, and only presented the most relevant ones in this article.

Second, the stitch numbers for PES differ slightly for PL1* patches, which seems like they are not objectively comparable. We justify this with the change in haptic quality when new material of a different type is introduced into the composition, which requires stitch numbers to be adjusted accordingly, hence, we went for comparable haptic quality.

Third, we did not test all our sensors to their full saturation, i.e., did not cover the entire working range. We did this since in our use case, 20 N was way beyond the expected upper limit; however, we noted especially during the tests with increasing actuation force that some variations perform badly beyond this value. This connects to a limitation of our Lycra-patches: offsets and hysteresis depending on actuation amplitude pose a challenge in general, since there seem to be temporal data (i.e., the degree of "past actuation") required to infer correct force and/or strain at all times. We plan to investigate this aspect in future work using a specially trained artificial neuronal network to act as a special filter. First steps into this direction already yielded promising results for compensating those temporal effects.

Finally, tests in harsh environmental conditions, such as in highly humid and extreme temperature scenarios, were not performed at this point. Related work showed that conductive polymer composites can be affected in particular by high humidity [37]; however, we expect that since this is a property of the material, the knitting structure does not have a profound influence in that regard. Since the sensing parts are entirely replaceable by similar products and our work was focusing on structural compositions and consistency benefits from adding Lycra material, we refrained from evaluating the specific materials that we used for our implementation, since we expect our results would reasonably translate to arbitrary resistive and conductive yarn.

GLOSSARY

The following is a short and arguably incomplete description of the terms used in the text; however, we refrain to go into more detail, since this should be sufficient for the scope of the article. For more details, refer to [1].

knit, tuck, float: Different stitch types performed by the needles. While a *knit* operation forms a new loop by pulling the new yarn through the currently held loop, a *tuck* just adds the yarn to the current loop, i.e., holding/securing the new yarn. In contrast, in a *float* (aka. "miss"), the yarn is guided behind the needle and not held at all.

wale, course: Terms describing the dimensions of a knit. Oversimplified but adequate for the scope of this article, wales and courses can be considered the "columns" and "rows" in a knit, when using matrices as an analogy.

REFERENCES

[1] D. J. Spencer, *Knitting Technology: A Comprehensive Handbook and Practical Guide*, 3rd ed. Sawston, U.K.: Woodhead Publishing, 2001.

[2] Y. Luo et al., "Heterogeneous strain distribution based programmable gated microchannel for ultrasensitive and stable strain sensing," *Adv. Mater.*, vol. 35, no. 2, Jan. 2023, Art. no. 2207141. [Online]. Available: https://onlinelibrary.wiley.com/doi/abs/10.1002/adma.202207141

[3] S. Li et al., "Bioinspired robot skin with mechanically gated electron channels for sliding tactile perception," *Sci. Adv.*, vol. 8, no. 48, Dec. 2022, Art. no. eade0720. [Online]. Available: https://www.science.org/doi/abs/10.1126/sciadv.ade0720

[4] X. Chen et al., "Scalable imprinting of flexible multiplexed sensor arrays with distributed piezoelectricity-enhanced micropillars for dynamic tactile sensing," *Adv. Mater. Technol.*, vol. 5, no. 7, Jul. 2020, Art. no. 2000046. [Online]. Available: https://onlinelibrary.wiley.com/doi/abs/10.1002/admt.202000046

[5] J. Shao, X. Chen, X. Li, H. Tian, C. Wang, and B. Lu, "Nanoimprint lithography for the manufacturing of flexible electronics," *Sci. China Technol. Sci.*, vol. 62, no. 2, pp. 175–198, Feb. 2019.

[6] O. Atalay, W. R. Kennon, and E. Demirok, "Weft-knitted strain sensor for monitoring respiratory rate and its electro-mechanical modeling," *IEEE Sensors J.*, vol. 15, no. 1, pp. 110–122, Jan. 2015.

[7] E. Ayodele et al., "Grasp classification with weft knit data glove using a convolutional neural network," *IEEE Sensors J.*, vol. 21, no. 9, pp. 10824–10833, May 2021.

[8] Y. Li, X. Miao, J. Y. Chen, G. Jiang, and Q. Liu, "Sensing performance of knitted strain sensor on two-dimensional and three-dimensional surfaces," *Mater. Design*, vol. 197, Jan. 2021, Art. no. 109273. [Online]. Available: https://www.sciencedirect.com/science/article/pii/S026412752030808X

[9] M. Åkerfeldt, A. Lund, and P. Walkenström, "Textile sensing glove with piezoelectric PVDF fibers and printed electrodes of PEDOT: PSS," *Textile Res. J.*, vol. 85, no. 17, pp. 1789–1799, Oct. 2015, doi: 10.1177/0040517515578333.

[10] X. Han, X. Miao, X. Chen, G. Jiang, and L. Niu, "Research on finger movement sensing performance of conductive gloves," *J. Engineered Fibers Fabrics*, vol. 14, Jan. 2019, Art. no. 155892501988762, doi: 10.1177/1558925019887622.

[11] S. Lee, Y. Choi, M. Sung, J. Bae, and Y. Choi, "A knitted sensing glove for human hand postures pattern recognition," *Sensors*, vol. 21, no. 4, p. 1364, Feb. 2021. [Online]. Available: https://www.mdpi.com/1424-8220/21/4/1364

[12] A. Grassi, F. Cecchi, M. Maselli, M. Röling, C. Laschi, and M. Cianchetti, "Warp-knitted textile as a strain sensor: Characterization procedure and application in a comfortable wearable goniometer," *IEEE Sensors J.*, vol. 17, no. 18, pp. 5927–5936, Sep. 2017.

[13] A. Liang, R. Stewart, and N. Bryan-Kinns, "Analysis of sensitivity, linearity, hysteresis, responsiveness, and fatigue of textile knit stretch sensors," *Sensors*, vol. 19, no. 16, p. 3618, Aug. 2019.

[14] X. Lin and B.-C. Seet, "A linear wide-range textile pressure sensor integrally embedded in regular fabric," *IEEE Sensors J.*, vol. 15, no. 10, pp. 5384–5385, Oct. 2015.

[15] S. D. Tohidi, A. Zille, A. P. Catarino, and A. M. Rocha, "Effects of base fabric parameters on the electro-mechanical behavior of piezoresistive knitted sensors," *IEEE Sensors J.*, vol. 18, no. 11, pp. 4529–4535, Jun. 2018.

[16] I. Wicaksono et al., "3DKnITS: Three-dimensional digital knitting of intelligent textile sensor for activity recognition and biomechanical monitoring," in *Proc. 44th Annu. Int. Conf. IEEE Eng. Med. Biol. Soc. (EMBC)*, Jul. 2022, pp. 2403–2409.

[17] H. Zhang, X. Tao, T. Yu, and S. Wang, "Conductive knitted fabric as large-strain gauge under high temperature," *Sens. Actuators A, Phys.*, vol. 126, no. 1, pp. 129–140, Jan. 2006. [Online]. Available: https://www.sciencedirect.com/science/article/pii/S0924424705005832

[18] B. Bozali, J. J. F. van Dam, L. Plaude, and K. M. B. Jansen, "Development of hysteresis-free and linear knitted strain sensors for smart textile applications," in *Proc. IEEE Sensors*, Oct. 2021, pp. 1–4.

[19] K. Yang, G.-L. Song, L. Zhang, and L.-W. Li, "Modelling the electrical property of 1×1 rib knitted fabrics made from conductive yarns," in *Proc. 2nd Int. Conf. Inf. Comput. Sci.*, vol. 4, May 2009, pp. 382–385.

[20] A. Ehrmann, F. Heimlich, A. Brücken, M. Weber, and R. Haug, "Suitability of knitted fabrics as elongation sensors subject to structure, stitch dimension and elongation direction," *Textile Res. J.*, vol. 84, no. 18, pp. 2006–2012, Nov. 2014, doi: 10.1177/0040517514548812.

[21] X. Chen, B. Li, Y. Qiao, and Z. Lu, "Preparing polypyrrole-coated stretchable textile via low-temperature interfacial polymerization for highly sensitive strain sensor," *Micromachines*, vol. 10, no. 11, p. 788, Nov. 2019.

[22] E. Ayodele, S. A. R. Zaidi, J. Scott, Z. Zhang, M. Hafeez, and D. McLernon, "The effect of miss and tuck stitches on a weft knit strain sensor," *Sensors*, vol. 21, no. 2, p. 358, Jan. 2021. [Online]. Available: https://www.mdpi.com/1424-8220/21/2/358

[23] X. Liang, H. Cong, Z. Dong, and G. Jiang, "Size prediction and electrical performance of knitted strain sensors," *Polymers*, vol. 14, no. 12, p. 2354, Jun. 2022. [Online]. Available: https://www.mdpi.com/2073-4360/14/12/2354

[24] S. Jang et al., "Printable wet-resistive textile strain sensors using bead-blended composite ink for robustly integrative wearable electronics," *Compos. B, Eng.*, vol. 210, Apr. 2021, Art. no. 108674. [Online]. Available: https://www.sciencedirect.com/science/article/pii/S1359836821000676

[25] Y. Teyeme, B. Malengier, T. Tesfaye, and L. van Langenhove, "A fabric-based textile stretch sensor for optimized measurement of strain in clothing," *Sensors*, vol. 20, no. 24, p. 7323, Dec. 2020. [Online]. Available: https://www.mdpi.com/1424-8220/20/24/7323

[26] D. De Rossi, F. Carpi, F. Lorussi, A. Mazzoldi, E. P. Scilingo, and A. Tognetti, "Electroactive fabrics for distributed, conformable and interactive systems," in *Proc. IEEE Sensors*, vol. 2, Jun. 2002, pp. 1608–1613.

[27] G. Semjonova, A. Davidovica, N. Kozlovskis, A. Okss, and A. Katashevs, "Smart textile sock system for athletes' self-correction during functional tasks: Formative usability evaluation," *Sensors*, vol. 22, no. 13, p. 4779, Jun. 2022. [Online]. Available: https://www.mdpi.com/1424-8220/22/13/4779

[28] R. Holm, *Electric Contacts: Theory and Application*, 4th ed. Berlin, Germany: Springer, 1967.

[29] L. Li, W. M. Au, K. M. Wan, S. H. Wan, W. Y. Chung, and K. S. Wong, "A resistive network model for conductive knitting stitches," *Textile Res. J.*, vol. 80, no. 10, pp. 935–947, Jun. 2010, doi: 10.1177/0040517509349789.

[30] S. Liu, C. Yang, Y. Zhao, X. M. Tao, J. Tong, and L. Li, "The impact of float stitches on the resistance of conductive knitted structures," *Textile Res. J.*, vol. 86, no. 14, pp. 1455–1473, Sep. 2016, doi: 10.1177/0040517514555798.

[31] N. Baribina, A. Oks, I. Baltina, and P. Eizentals, "Comparative analysis of knitted pressure sensors," in *Proc. Eng. Rural Develop.*, May 2018, pp. 1599–1604.

[32] R. Aigner, M. A. Haberfellner, and M. Haller, "spaceR: Knitting ready-made, tactile, and highly responsive spacer-fabric force sensors for continuous input," in *Proc. 35th Annu. ACM Symp. User Interface Softw. Technol.* New York, NY, USA: Association for Computing Machinery, Oct. 2022, pp. 1–15, doi: 10.1145/3526113.3545694.

[33] A. Pointner, T. Preindl, S. Mlakar, R. Aigner, M. A. Haberfellner, and M. Haller, "Knitted force sensors," in *Adjunct Proc. 35th Annu. ACM Symp. User Interface Softw. Technol.* New York, NY, USA: Association for Computing Machinery, Oct. 2022, pp. 1–3, doi: 10.1145/3526114.3558656.

[34] C. Isaia, S. A. McMaster, and D. McNally, "Study of performance of knitted conductive sleeves as wearable textile strain sensors for joint motion tracking," in *Proc. 42nd Annu. Int. Conf. IEEE Eng. Med. Biol. Soc. (EMBC)*, Jul. 2020, pp. 4555–4558.

[35] J. Ou, D. Oran, D. D. Haddad, J. Paradiso, and H. Ishii, "SensorKnit: Architecting textile sensors with machine knitting," *3D Printing Additive Manuf.*, vol. 6, no. 1, pp. 1–11, Mar. 2019, doi: 10.1089/3dp.2018.0122.

[36] K. M. B. Jansen, "Performance evaluation of knitted and stitched textile strain sensors," *Sensors*, vol. 20, no. 24, p. 7236, Dec. 2020. [Online]. Available: https://www.mdpi.com/1424-8220/20/24/7236

[37] C. Cochrane, V. Koncar, M. Lewandowski, and C. Dufour, "Design and development of a flexible strain sensor for textile structures based on a conductive polymer composite," *Sensors*, vol. 7, no. 4, pp. 473–492, Apr. 2007. [Online]. Available: https://www.mdpi.com/1424-8220/7/4/473